Supporting Information (Ichikawa et al.)

SI METHODS

Tracer labeling. Under chloral hydrate anesthesia (350 mg/kg body weight, i.p.), biotinylated dextran amine (BDA, molecular weight, 10,000; Invitrogen, Carlsbad, CA, USA) was injected into the inferior olivary nucleus by the dorsal approach, as reported previously (7). After 48 h of survival for postnatal day 7 (P7), P9 and P12 mice, or 72 h for P15, P20, P30, and P40 mice, transcardial perfusion was conducted under chloral hydrate anesthesia using 4% paraformaldehyde in 0.1 M phosphate buffer (PB, pH7.4) for light microscopy or 0.1% glutaraldehyde/4% paraformaldehyde in PB for pre-embedding immunogold electron microscopy. Cerebella were removed quickly and immersed overnight in the same fixative, followed by rinsing in PB for at least 1 day. All analyses were done on lobules 4/5 and 6 of the left vermal cerebellum.

Lentivirus experiment. We used the lentiviral vector system pseudotyped with vesicular stomatitis virus glycoprotein (VSVG) (48). The viral vectors were designed to express GFP or GFP and mouse mGluR1α under control of the murine embryonic stem cell virus promoter or a truncated L7 promoter comprising 1 kb of the original Purkinje cell-specific L7 promoter (49). For bicistronic expressions of GFP and mGluR1α, cDNA encoding mouse mGluR1α was fused in frame with cDNA encoding GFP via picornavirus self-cleaving P2A peptide sequence. For the production of lentiviral vectors, the four-plasmid mixture consisted of pCAG-kGP1R, pCAG4-RTR2, pCAGGS-VSVG, and pCL20c-based main lentivector plasmid was co-transfected into human embryonic kidney (HEK) 293T cells using a calcium phosphate precipitation

method. HEK293T cells were cultured in DMEM (D5796; Sigma) supplemented with 10% fetal bovine serum (Cell Culture Bioscience), 1× penicillin/streptomycin (P4333; Sigma), 1 mM sodium pyruvate (S8636; Sigma), 1× MEM non-essential amino acid solution (M7145; Sigma), and 1× GlutaMAX (#35050061; Life Technologies) at 37°C in a 10% CO_2 atmosphere. 16 h after transfection, culture medium was replaced with Ultraculture (12-725F, Lonza) supplemented with 1× GlutaMAX. 40 hours after transfection, viral supernatants were collected, filtrated through 0.45 μm membranes, and concentrated at 6000× g for 16 h. Viral particles were suspended with PBS ($1.0 \times 10^{4\text{-}8}$ transducing unit/ml).

Virus suspension (0.5 μl) was injected by air pressure into the vermis of cerebellar lobules VI–VII at P1 under hypothermal anesthesia. At P15 and P20, mice were anesthetized and fixed by transcardial perfusion with 4% paraformaldehyde in 0.1M PB. For lentivirus-mediated mGluR1α transfection, virus suspension (0.5 μl) was injected by air pressure into the vermis of cerebellar lobules V–VI in mGluR1-KO mice at P20 under chloral hydrate anesthesia (350 mg/kg body weight, i.p.). After 20 days of survival, mice were anesthetized and fixed by transcardial perfusion with 4% paraformaldehyde in 0.1M PB.

Electrophysiology. Parasagittal cerebellar slices (250 μm thickness) were prepared from C57BL/6 mice at P14 to P20 as described previously (4). Whole-cell recordings were made from visually identified PC somata using an upright microscope (BX50WI, Olympus, Tokyo, Japan). All experiments were carried out at room temperature. Resistances of patch pipettes were 2–3 MΩ when filled with an intracellular solution composed of (in mM): 60 CsCl, 10 Cs D-gluconate, 20 TEA-Cl, 20 BAPTA, 4 $MgCl_2$, 4 ATP and 30 HEPES (pH 7.3, adjusted with CsOH). The composition of the standard

bathing solution was (in mM): 125 NaCl, 2.5 KCl, 2 $CaCl_2$, 1 $MgSO_4$, 1.25 NaH_2PO_4, 26 $NaHCO_3$, 20 glucose and 0.01 bicuculline, bubbled with 95 % O_2 and 5 % CO_2. The membrane potential was always held at -70 mV. For recording of mEPSCs, tetrodotoxin (0.5 μM) was added to the standard bathing solution. To enhance the frequency of mEPSCs, the external 2 mM Ca^{2+}/1 mM Mg^{2+} was replaced with 4 mM Ca^{2+}/0 mM Mg^{2+}. To record quantal EPSCs arising from CF synapses, CFs were stimulated with a glass microelectrode in the external solution in which 2 mM Ca^{2+}/1 mM Mg^{2+} was replaced with 1 mM Sr^{2+}/2 mM Mg^{2+}. Because a Group II mGluR agonist, DCG IV, is an agonist of NMDA receptors, R-CPP (5 μM) was always supplemented in the Sr^{2+}-containing external solution. Ionic currents were recorded with an Axopatch 1D (Molecular Devices, Sunnyvale, CA, USA) patch clamp amplifier. The signals were filtered at 3 kHz and digitized at 40 kHz for recording evoked EPSCs. On-line data acquisition and off-line data analysis were performed using PULSE and PATCHMASTER software (HEKA). Miniature EPSCs were analyzed with the Mini Analysis Program (ver. 6.0.7, Synaptosoft Inc., Decatur, GA, USA).

SI Figure Legends

Fig. S1. *A–F*. Bright-field micrographs of biotinylated dextran amine (BDA)-labeled climbing fibers (CFs) used for ultrastructural analysis from P7 to P30. For ultrastructural reconstruction, we selected BDA-labeled CFs whose trajectories could be traced from Purkinje cell (PC) somata to the tips of CFs. Red and blue arrows indicate approximate portions of the most distal CF synapses (CFd) and the most proximal parallel fiber synapses (PFp) shown in Fig. S1*G–X*. After taking these micrographs, sections were subjected to pre-embedding silver-enhanced immunogold microscopy for VGluT1 to label PF terminals, and embedded in Epon812. Asterisks indicate PC somata. *G–X*. Electron micrographs showing the most distal CF synapses and the most proximal PF synapses at P7 (*G, H*), P9 (*I, J*), P12 (*K, L*), P15 (*M–P*), P20 (*Q–T*), and P30 (*U–X*). Boxed regions in *G–L* are enlarged in insets, while those in *M, N, Q, R, U,* and *V* are enlarged in *O, P, S, T, W,* and *X*, respectively. Insets in *G*, *I*, and *K* and closer views of *O*, *S*, and *W* show the most distal CF synapses (CFd) labeled with BDA tracer (diffuse DAB precipitates). Insets in *H*, *J*, and *L* and closer views of *P*, *T*, and *X* show the most proximal PF synapses (PFp) labeled for VGluT1 (metal particles). Arrows indicate the coexistence of CFd with PF synapses or of PFp with CF synapses (CF). Pairs of arrowheads indicate both edges of the postsynaptic density. PC dendrites or somata are pseudocolored in green. Note reduced calibers of CFd- and PFp-associated PC dendrites owing to distal elongation of CF territory or distal retraction of PF territory, respectively, during early postnatal period. Also note that the most distal CF synapses at P7 are observed at apical portions of PC somata or somatodendritic border. Scale bars: *A–F*, 10 μm; *G–X*, 500 nm.

Fig. S2. Electron micrographs showing synapses and free spines on PC dendrites at P15. *A,* CF synapse on a PC spine (Sp), identified by diffuse dark precipitates for the anterograde tracer BDA in the presynaptic terminal and an asymmetrical contact characterized by a thick postsynaptic density (arrowheads). *B,* PF synapses on PC spines, identified by metal particle labeling for VGluT1 and asymmetrical contacts (arrowheads). *C,* GABAergic synapse on a dendritic shaft of PC, identified by metal particle labeling for VIAAT and a symmetrical contact (arrowheads). *D,* Symmetrical synapse on a right PC spine. *E,* GABAergic synapse on a PC spine, identified by metal particle labeling for VIAAT and a symmetrical contact (arrowheads). *F,* Serial images of a free spine, which is surrounded by Bergmann glia and lacking synaptic contact. Scale bars, 500 nm.

Fig. S3. Reconstructed dendritic innervation in wild-type PCs at P7 (*A*), P9 (*B*), P12 (*C*), P15 (*D*), P20 (*E*) and P30 (*F*). CF synapses (yellow circles on red lines) and PF synapses (blue circle) are shown to the right of PC somata and dendrites (gray), while GABAergic spine-type synapses (green square) and free spines (black square) are to the left of dendrites. See also Fig. 2*A*-*F*.

Fig. S4. Schematic showing how the path length of curving and leaning dendrites was calculated. Assuming that dendrites are cylindrical, the red triangle defined by the long (D_L) and short (D_S) diameters of dendritic profiles is similar in shape to the yellow triangle defined by the path length (L) and section thickness (t). Therefore, the path length in each section is calculated as $D_L/D_S \times t$, and is summed to obtain the total path length of the CF or PF territory in a given PC.

Fig. S5. Electrophysiological analysis of miniature EPSCs (mEPSCs) in PCs. *A*, Sample traces of mEPSCs at P15 (upper) and P20 (lower). Representative events (red arrow heads) are shown in higher time and current resolutions on the right. *B*, Normalized frequency distribution histograms for the 10–90 % rise times of mEPSCs sampled at P14–P16 (blue, n = 31) and at P18–P20 (pink, n = 23). The normalized frequency of mEPSCs was higher at P14–P16 than at P18–P20 for the rise times of 0.4, 0.6, and 2.6 ms bins, and vice versa for 1.8 ms bin ($p < 0.05$, t-test). In the following analyses, we focused on the events with the rise times of 0.2–0.6 ms that are considered to arise from synapses on the proximal portions of PC dendrites. A rationale for this notion is that the rise times of quantal EPSCs arising from CFs, which form synapses on proximal PC dendrite, were shorter than 1 ms for most of the events (see *E*). *C*, Incidence of mEPSCs with rise times of 0.2–0.6 ms at P14–P16 was significantly higher than that at P18–P20 (t-test, $p = 0.00844$). *D*, Asynchronous quantal EPSCs arising from CFs recorded in the external solution containing Sr^{2+} (1 mM) from PCs at P14–P16. (left) Representative traces of EPSCs. Events were sampled during 500 ms period after the CF stimulation. The red arrow indicates time points when CFs were stimulated. Representative events (red arrowhead) are shown in higher time and current resolutions on the right. (right) Normalized frequency distribution histograms for the 10–90 % rise times of quantal EPSCs at P14–P16 (n = 10). Note that the rise time was faster than 1 ms for most of the events. *E*, Normalized frequency distribution histograms for the 10–90 % rise times of mEPSCs in the absence (open circles) and the presence (filled circles) of L-AP4 (50 μM) at P14–P16 (upper, n = 8) and at P18-P20 (lower, n= 5). Bar graphs on the right of

the histograms show the incidence of mEPSCs with rise times of 0.2–0.6 ms in the absence (open circles) and the presence (filled circles) of L-AP4 (50 μM). Note that L-AP4 significantly reduced the incidence at P14-P16 (upper, paired-t test, n = 8, p = 0.0044) but not at P18-P20 (lower, n = 5, p = 0.08). Histograms for L-AP4 treatment are normalized to the number of events elicited in the control solution. *F*, Incidence of quantal EPSCs arising from CFs was not affected by L-AP4 (50 μM) but markedly suppressed by the group II mGluR agonist DCG IV (1 μM) that are known to suppress CF-mediated EPSCs (50). (One-way ANOVA with Holm-Sidak post hoc test, control n = 8, L-AP4 n = 8, DCG IV n = 6, $p < 0.001$). Three sample traces (left) and summary bar graph (right) showing the effects of L-AP4 (50 μM) and DCG-IV (1 μM). Red arrows indicate time points when CFs were stimulated. For *B, C, D, E* and *F*, values are expressed as mean ± SEM. * $p < 0.05$, ** $p < 0.01$.

Fig. S6. CF and PF innervation in mGluR1-KO and PKCγ-KO mice. *A–D*, Triple fluorescent labeling for CFs (red, BDA tracer labeling), PF terminals (blue, VGluT1 immunofluorescence) and PCs (green, calbindin immunofluorescence) at P15 (*A, C*) and P30 (*B, D*) in mGluR1-KO (*A, B*) and PKCγ-KO (*C, D*) mice. Arrowheads indicate the tip of the CF projection, while arrows indicate the somatodendritic border of PCs. *E–H*, Reconstructed dendritic innervation in three PCs at P15 (*E, G*) and P30 (*F, H*) in mGluR1-KO (*E, F*) and PKCγ-KO (*G, H*) mice. See legends in Fig. 1A-F and Fig. 2A-F. Scale bars, 10 μm.

Fig. S7. Reconstructed dendritic innervation in mGluR1-KO (*A*) and mGluR1α-rescued (*B*) PCs. See also Fig. 5*H, I*.

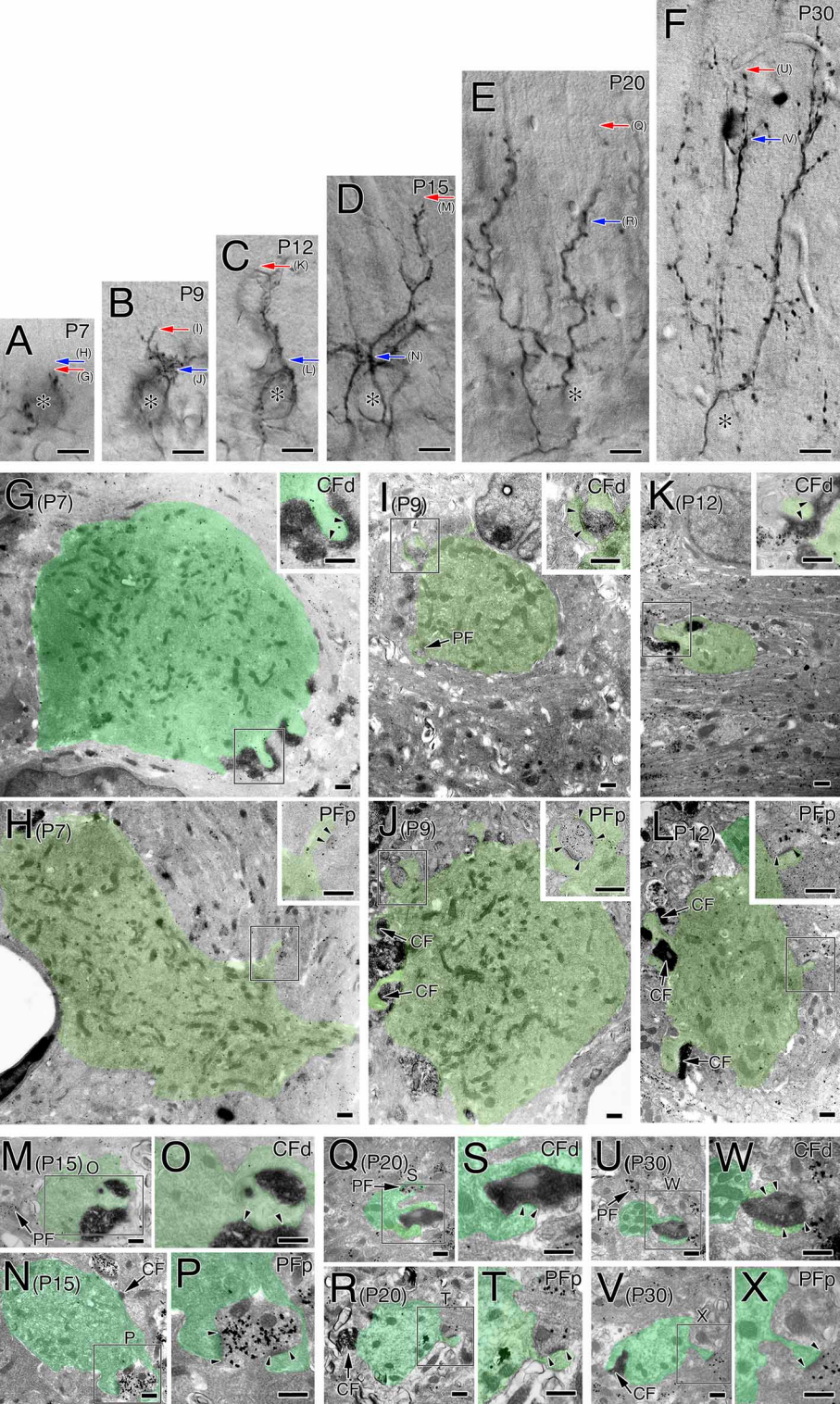
A
P7
(H)
(G)
B
P9
(I)
(J)
C
P12
(K)
(L)
D
P15
(M)
(N)
E
P20
(Q)
(R)
F
P30
(U)
(V)
G (P7)
CFd
H (P7)
PFp
I (P9)
CFd
PF
J (P9)
PFp
CF
CF
K (P12)
CFd
L P12)
PFp
CF
CF
CF
M (P15)
O
PF
O
CFd
N (P15)
CF
P
P
PFp
Q (P20)
S
PF
S
CFd
R (P20)
T
CF
T
PFp
U (P30)
W
PF
W
CFd
V (P30)
X
CF
X
PFp

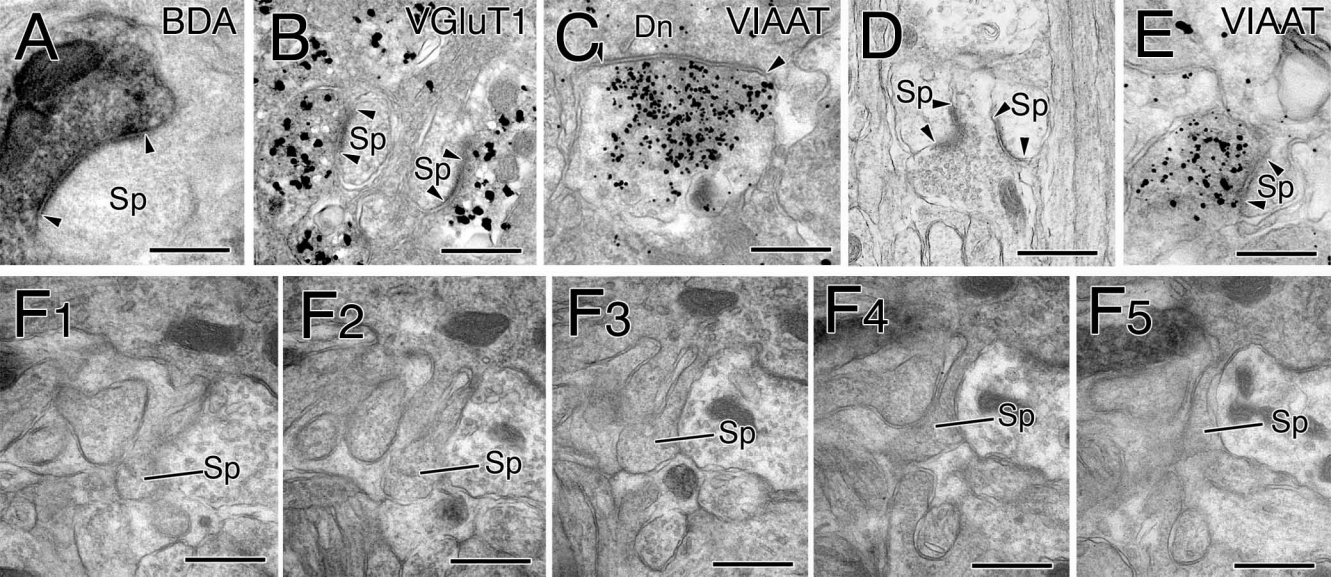
A
BDA
Sp
B
VGluT1
Sp
Sp
C
Dn
VIAAT
D
Sp
Sp
E
VIAAT
Sp
F1
Sp
F2
Sp
F3
Sp
F4
Sp
F5
Sp

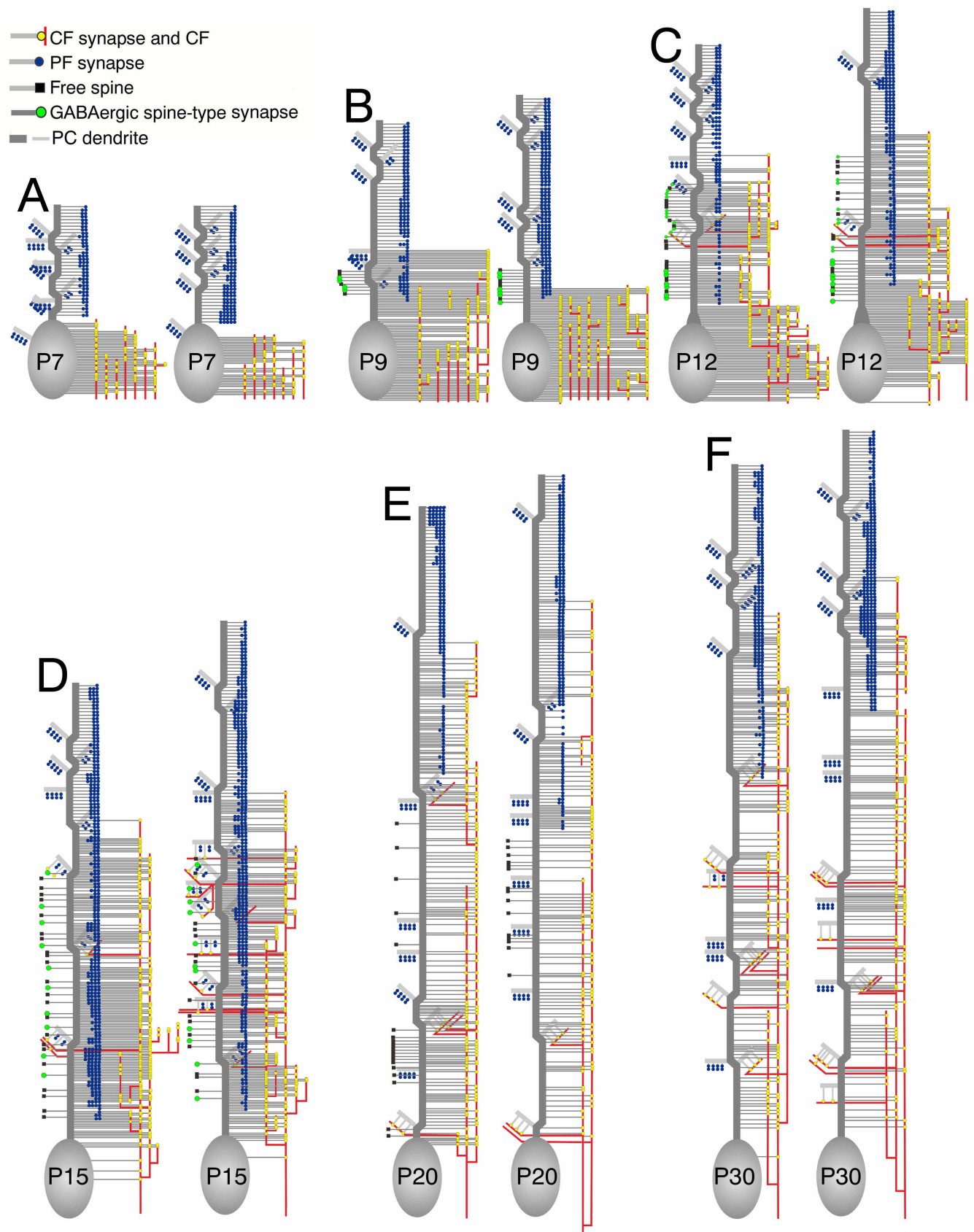
CF synapse and CF
PF synapse
Free spine
GABAergic spine-type synapse
PC dendrite
A
P7
P7
B
P9
P9
C
P12
P12
D
P15
P15
E
P20
P20
F
P30
P30

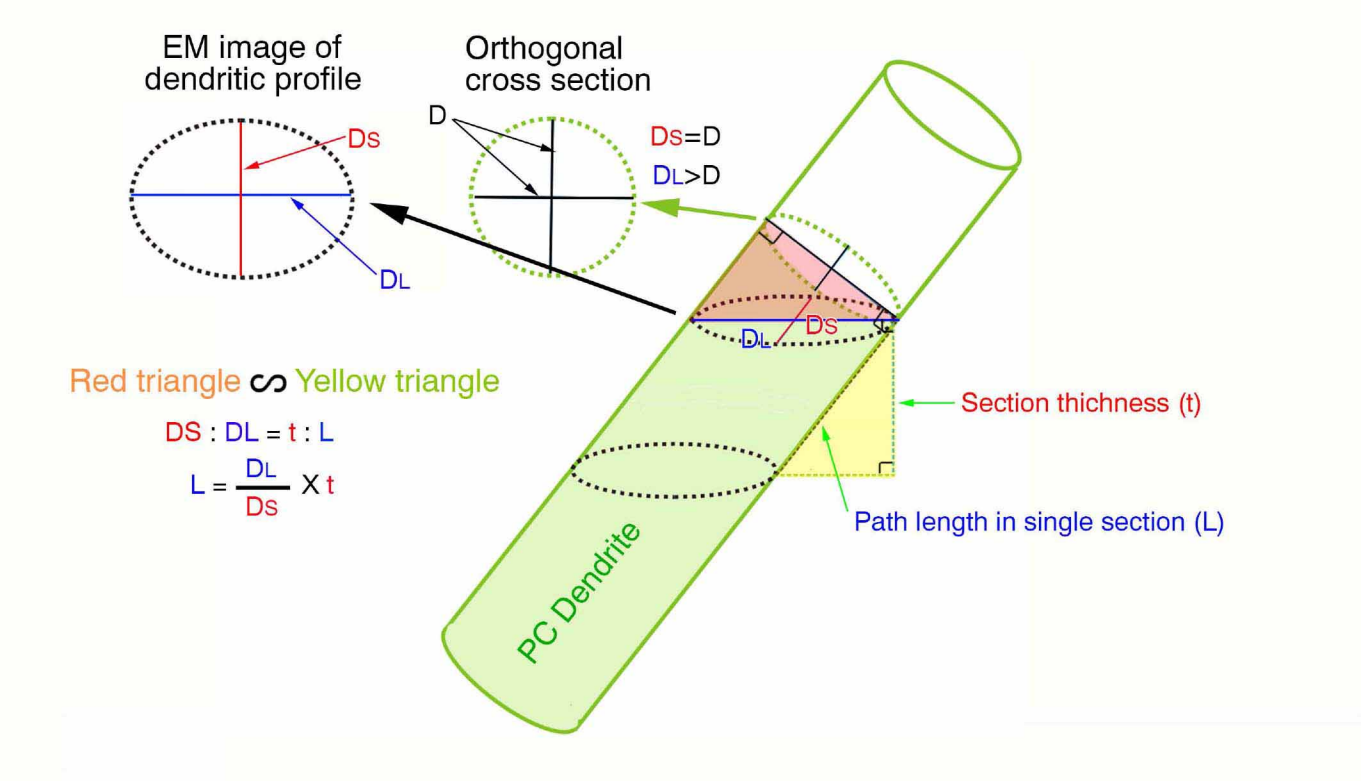
EM image of dendritic profile
Ds
DL
Orthogonal cross section
D
Ds=D
DL>D
DL
Ds
Red triangle ∽ Yellow triangle
DS : DL = t : L
L = DL / Ds X t
Section thichness (t)
Path length in single section (L)
PC Dendrite

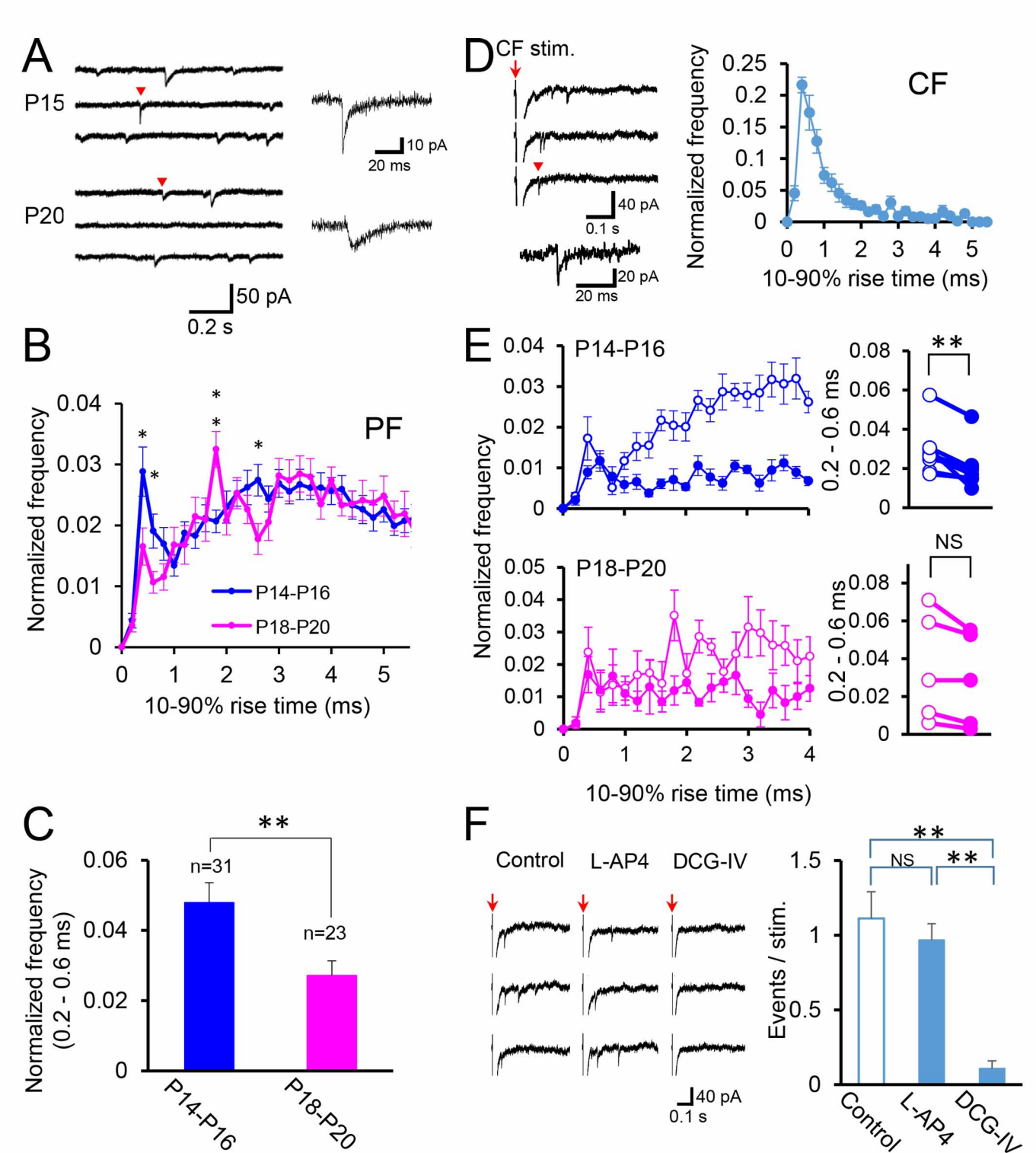
A
P15
P20
10 pA
20 ms
50 pA
0.2 s
B
PF
Normalized frequency
P14-P16
P18-P20
10-90% rise time (ms)
C
Normalized frequency (0.2 - 0.6 ms)
n=31
n=23
P14-P16
P18-P20
D
CF stim.
40 pA
0.1 s
20 pA
20 ms
CF
Normalized frequency
10-90% rise time (ms)
E
P14-P16
P18-P20
Normalized frequency
0.2 - 0.6 ms
NS
10-90% rise time (ms)
F
Control
L-AP4
DCG-IV
40 pA
0.1 s
Events / stim.
NS
Control
L-AP4
DCG-IV

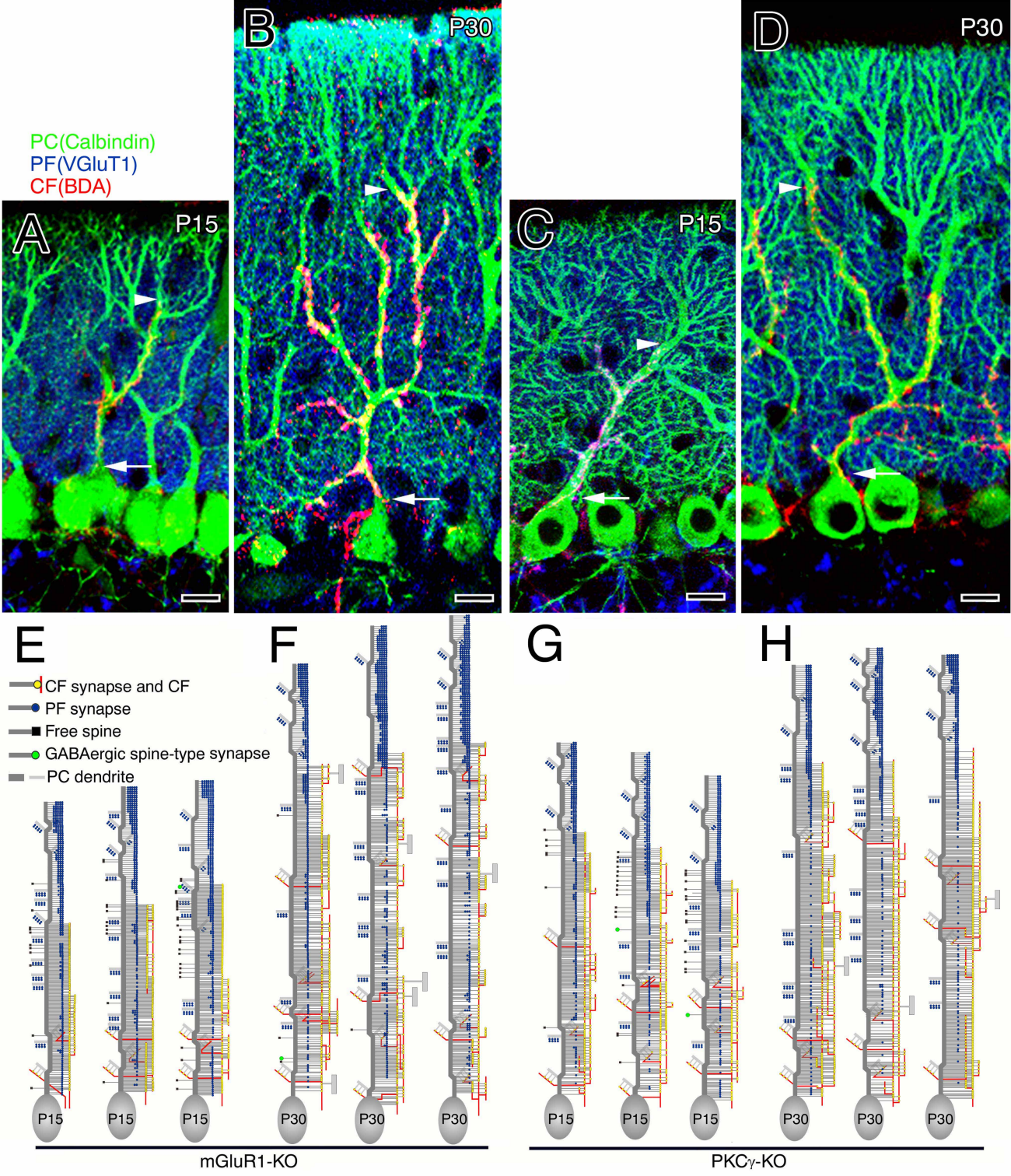
PC(Calbindin)
PF(VGluT1)
CF(BDA)
A
P15
B
P30
C
P15
D
P30
E
F
G
H
CF synapse and CF
PF synapse
Free spine
GABAergic spine-type synapse
PC dendrite
P15
P15
P15
P30
P30
P30
P15
P15
P15
P30
P30
P30
mGluR1-KO
PKCγ-KO

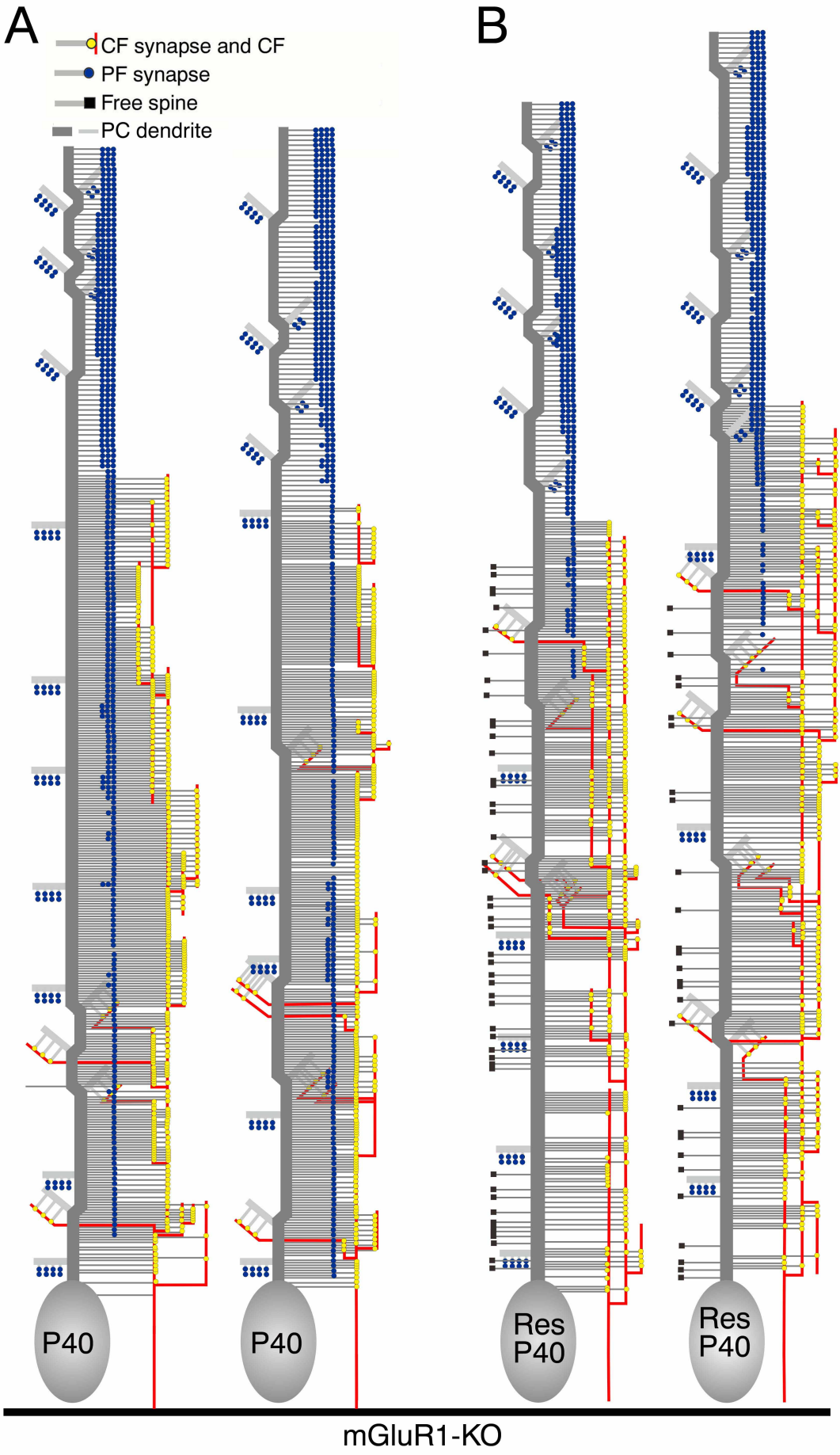
A
CF synapse and CF
PF synapse
Free spine
PC dendrite
P40
P40
B
Res
P40
Res
P40
mGluR1-KO